Changes in seal capacity of fractured claystone caprocks induced by dissolved and gaseous CO2 seepage

Muriel Andreani, Philippe Gouze, Linda Luquot, P. Jouanna

Changes in seal capacity of fractured claystone caprocks induced by dissolved and gaseous CO_2 seepage

M. Andreani,[1] P. Gouze,[1] L. Luquot,[1] and P. Jouanna[1]

Received 25 April 2008; revised 11 June 2008; accepted 17 June 2008; published 31 July 2008.

[1] Claystone caprocks are often the ultimate seal for CO_2 underground storage when residual CO_2 gas reaches the reservoir top due to buoyancy. Permeability changes of a fractured claystone due to seepage of CO_2-enriched brine and water vapor-saturated CO_2 gas are investigated. Results show that brine flow induces a large porosity increase (up to 50%) in the vicinity of the fracture due to dissolution of calcite and quartz, while permeability remains unchanged. Conversely, cyclic flows of CO_2-brine and CO_2-gas increase the fracture aperture abruptly after each gas flow period, producing a progressive decrease of the caprock seal capacity. Aperture increase is controlled by decohesion of the clay framework within a micrometer-scale-thick layer induced by CO_2-gas acidification. Results show that hydraulic aperture increases linearly with duration of the preceding CO_2-brine flow period, emphasizing the kinetic control of the quartz grains dissolution during the brine flow periods. **Citation:** Andreani, M., P. Gouze, L. Luquot, and P. Jouanna (2008), Changes in seal capacity of fractured claystone caprocks induced by dissolved and gaseous CO_2 seepage, *Geophys. Res. Lett.*, *35*, L14404, doi:10.1029/2008GL034467.

1. Introduction

[2] Geological CO_2 sequestration in sedimentary reservoirs is a main option for reducing atmospheric overload. After injection as a supercritical fluid, massive sequestration of CO_2 in solution requires extensive renewal of the water in contact with the supercritical CO_2 which will usually remain in the reservoir during thousands of years after injection. Supercritical CO_2 will migrate upward by density-driven motion towards regions with lower temperature and pressure, and eventually transform to gas [*Pruess and Garcia*, 2002]. The critical issue is the sealing integrity of the reservoir caprock. Caprocks are often claystone layers with a low-permeability matrix, where CO_2 seepage may occur according to three main physical mechanisms: diffusion, capillary breakthrough and pressure-driven flow through localized hydraulic discontinuities. Diffusion and capillary-driven flow are slow processes compared to pressure-driven flow in fractures [*Hildenbrand and Krooss*, 2003]. Pressure recovery during CO_2 injection and tectonic events may reactivate pre-existing weaknesses inherited from reservoir production periods and create new fractures in the caprock. Then, the differential pressure between the reservoir and the caprock-overlaying aquifers will promote upward flows of either CO_2-enriched water, sub- or super-critical CO_2, or a diphasic mixture of water and CO_2, depending on the hydrodynamics of the reservoir and on the gas-to-water ratio. Then, rock alteration is expected due to the thermodynamic non-equilibrium between reservoir fluids and caprock minerals, mainly clay, carbonate and silica.

[3] So far, claystone reactivity was studied experimentally in alkaline conditions in view of radioactive waste disposal, while investigation of claystone alteration by CO_2-rich fluids was mainly limited to numerical modeling [e.g., *Gherardi et al.*, 2007]. However, numerical models are very sensitive to uncertainties of reaction-controlling parameters in clay-rich rocks. In particular, kinetic rate constants, reactive surface-areas and permeability of fracture networks are poorly known. Moreover claystones generally do not form continuous mineral clusters, where mass transfers are difficult to simulate. Finally, clay swelling or shrinkage due to ion exchange may induce mechanical alteration that, in turn, modifies the caprock properties.

[4] In this letter, the issue of whether such phenomena increase or decrease impact of pre-existing hydraulic discontinuities on caprock sealing properties is addressed. For that purpose, flow cycles of CO_2-enriched reservoir water (brine) and water vapor-saturated CO_2 gas through a fractured claystone sample are reproduced at laboratory scale.

2. Experimental Method

2.1. Rock Material and Sample Preparation

[5] The indurated argillaceous material used in this study comes from the Upper Toarcian formation of Tournemire (France) whose composition is close to the Paris Basin caprocks where French CO_2 pilot injection is scheduled. A cylinder of diameter $D = 9$ mm and length $L = 15$ mm was sampled from a borehole core. The mineralogical composition of the material[1], provided by *Sibai et al.* [1993] and confirmed by X-ray diffraction and SEM investigations, is in volume percent: 25% calcite, 2% siderite, 25% quartz, 45% clay minerals and 3% pyrite, with an overall density of 2.6. The clay fraction composition is: 24% kaolinite, 10% micas (muscovite), 10% interstratified illite/smectite and 1% chlorite. The total Hg-accessible porosity is $\phi = 7.1\%$ and the pore diameters are less than 20 nm. The specific surface-area, $S_s = 21.6 \times 10^3$ $m^2.kg^{-1}$, was measured by nitrogen gas absorption at 77 K. SEM imaging of rock microstructure shows that quartz and calcite grains of some 10 μm are disseminated in the clayey matrix[1]. Carbonates are also present locally as pervasive cements around clay clusters. Semi-quantitative analyses using EDS-SEM show that the clay fraction contains principally K and Fe, and, to a lesser extent, Mg and Na (Table 1). The Ca content is very low ($\leq$1 wt %). A planar fracture is obtained by sawing the

[1]Géosciences Montpellier, CNRS, Montpellier, France.

0094-8276/08/2008GL034467

[1]Auxiliary material data sets are available in the HTML. doi:10.1029/2008GL034467.

Table 1. Water and Claystone Compositions[a]

	Ca	Mg	K	Na	Fe	Al	Si	pH	Ionic Strength
Claystone-equilibrated water (mol/kg)	6.05×10^{-4}	6.80×10^{-5}	6.87×10^{-5}	1.38×10^{-4}	1.29×10^{-6}	2.93×10^{-6}	7.38×10^{-5}	7.7	9.3×10^{-5}
Reservoir water (brine) (mol/kg)	1.57×10^{-2}	8.95×10^{-3}	5.10×10^{-3}	1.03	3.05×10^{-7}	4.08×10^{-7}	1.21×10^{-6}	6.8	1.08
Res. water + PCO_2 = 0.12 MPa (mol/kg)	1.57×10^{-2}	8.95×10^{-3}	5.10×10^{-3}	1.03	3.05×10^{-7}	4.08×10^{-7}	1.21×10^{-6}	5.1	1.08

	Ca	Mg	K	Na	Fe	Al	Si	Ti	S	Cl
Initial fracture surface (wt%)	11.04	2.39	6.27	0.55	6.88	22.58	47.44	1.22	1.49	0.18
Final fracture surface (wt%)	1.30	2.51	7.12	0.93	7.69	23.74	53.02	1.31	1.34	1.03
Clay-dominated zone (wt%)	1.08	2.78	7.80	2.27	5.95	28.67	50.01	0.93	0.24	0.27

[a]EDS-SEM data for fracture surfaces and clay-dominated zone are averaged over three 250^2 μm^2 and three 5^2 μm^2 areas, respectively.

cylinder in two halves that are subsequently tied together by their edges with fiberglass-loaded epoxy resin (Figure 1). The inlet and outlet areas of the samples, except for the fracture void, are covered by a glued plastic sheet to avoid chemical reaction outside the fracture.

2.2. Experimental Protocol

[6] Tests are performed at 25°C in a flow-through reactor[1]. The sample is placed in a silicon jacket and positioned in a confinement cell where pressure is maintained equal to the inlet fluid pressure. Water flow rate is controlled by a motorized dual-piston pump. The inlet fluid is enriched in CO_2 up to a partial pressure P_{CO_2} = 0.12 MPa by CO_2 gas bubbling in a pressurized stirred vessel where pH is continuously recorded. The outlet pressure is maintained slightly higher than 0.12 MPa using a back-pressure controller to prevent CO_2 gassing in the circuit. Effluent pH is recorded continuously upstream of the pressure controller. Cation concentrations in the effluent are measured recurrently using ICP-AES (with a cumulated uncertainty <10%.) after acidification with HNO_3.

[7] Owing to the very low matrix permeability of the rock ($\sim 10^{-21}$ m^2 [*Boisson et al.*, 2001]), the measured permeability is that of the fracture. For laminar flow in a planar fracture, the fracture hydraulic aperture, a_H, is calculated from the recorded pressure drop across the sample[1], ΔP, using the cubic law approximation $a_H = (12Q.\mu.L./w.\Delta P)^{1/3}$ with Q the flow rate and μ the fluid dynamic viscosity. By analogy with Darcy's law, the permeability is $k = a_H^2/12$.

2.2.1. Sample Saturation

[8] First, a claystone-equilibrated water is prepared by mixing powdered claystone with distilled water for two months. Repeated analysis of the fluid shows that thermodynamic equilibrium is achieved after five weeks. Second, this water (previously filtered at 0.2 μm) is injected in the sample until saturation (i.e. $P_{H_2}0$ = 0.12 MPa). Saturation is determined when a_H decreases to a constant value after 12 days (a_H = 48.5 μm, $k = 1.9 \times 10^{-10}$ m^2). For details, see auxiliary materials.[1]

2.2.2. Cyclic Percolation

[9] Typical carbonate-reservoir brine is made using distilled water and laboratory-grade salts (Table 1). This brine is subsequently saturated with CO_2 at a partial pressure P_{CO_2} = 0.12 MPa and injected in the sample at a constant flow rate $Q = 6.94 \times 10^{-9}$ $m^3.s^{-1}$ (0.6 $L.day^{-1}$). This value is determined in order to measure ΔP accurately, while corresponding to very smooth laminar flow (Reynolds number ≈1.5) for avoiding mechanical alteration processes. Water-saturated CO_2 gas injection is performed at the same flow rate. Hereafter, CO_2-enriched brine and water-saturated CO_2 are called CO_2-brine and CO_2-gas, respectively. Each cycle includes a period of CO_2-brine flow followed by a period of CO_2-gas flow. Two experiments using similar samples are performed to check reproducibility. Experiments 1 and 2, including four and two CO_2-brine/CO_2-gas cycles respectively, display similar results summarized in Figure 2.

3. Results

[10] Results are reported in terms of hydraulic aperture and outlet fluid composition changes, for the 4-cycles

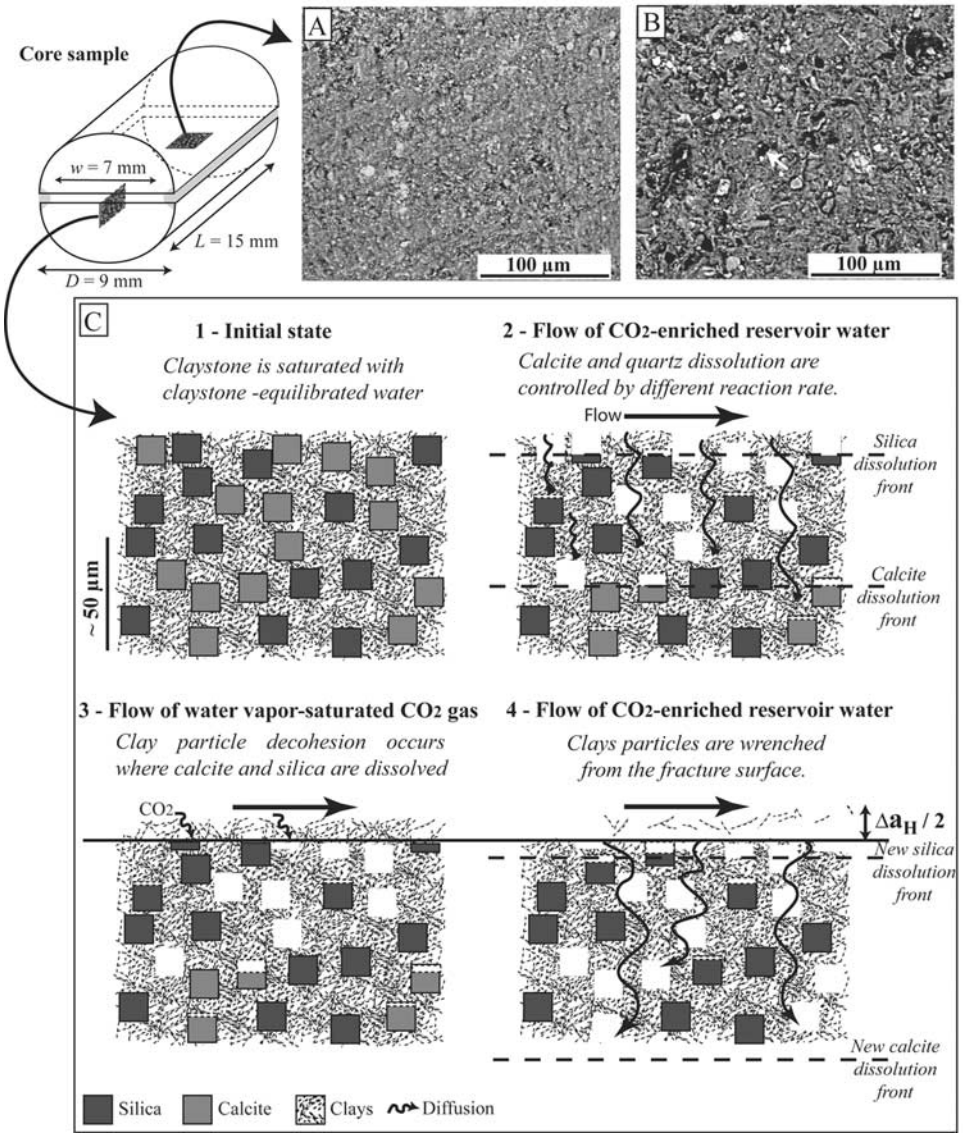

Figure 1. EDS-SEM images (a) of the initial fracture surface and (b) at the end of experiment 1. (c) Schematic representation of the mechanisms proposed for explaining fracture evolution during cyclic CO_2-brine and CO_2-gas flows.

experiment 1 that lasted 33 days (Figure 3). Notations F_i and G_i designate CO_2-brine and CO2-gas flow periods of cycle number i.

[11] After each period of gas flow, a_H increases by a variable amount ranging from 5.8 μm (after G_1) to 1 μm (after G_2 and G_3), while a_H remains constant during CO_2-brine flow period (F_1 to F_5). The cumulated increase in fracture aperture is 11.6 μm, which corresponds to an increase of 24%. Final permeability is 3×10^{-10} m^2. For the two experiments, the increase of a_H at the beginning of each CO_2-brine flow period scales linearly with the duration of the preceding CO_2-brine flow period $\Delta t^{(F_{i-1})}$ (circles in Figure 2), but is independent of the duration of the preceding CO_2-gas-flow period $\Delta t^{(G_{i-1})}$ (triangles in Figure 2).

[12] After the first CO_2-brine injection (F_1, $t = 280$ hours), K concentration increases progressively up to the reservoir K composition and then remains relatively stable until the end of the experiment, except for short peaks at the beginning of each CO_2-brine flow period (Figure 3). By contrast, Ca concentration of the outlet fluid rises above the Ca inlet fluid composition and finally tends asymptotically to the inlet fluid composition, indicating that Ca is continuously released from the sample. Chemical data (Table 1) indicate that Ca is mainly localized in calcite grains (average size 10 μm). Consequently, the release of Ca corresponds to calcite dissolution, which is in agreement with the change of the outlet fluid pH. Calcite dissolution is also corroborated by comparing the surface microstructures and Ca concentration map of the fracture surface before and after the whole experiment (Figures 1a and 1b, Table 1). The total volume of calcite dissolved during the experiment is 0.038 cm^3 according to the outlet fluid, whereas the fractured sample initially contained 0.246 cm^3 of calcite according to the mean mineralogical composition of the claystone. Consequently, 15.5% of the initial calcite is dissolved during the experiment with half of this fraction during period F_1.

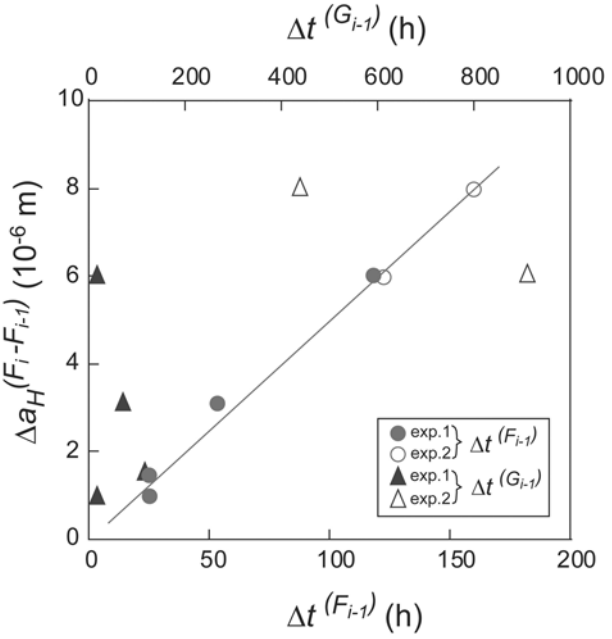

Figure 2. Hydraulic aperture increase $\Delta a_H^{(F_i - F_{i-1})}$ between two successive CO_2-brine flow periods F_{i-1} and F_i versus $\Delta t^{(F_{i-1})}$, the previous CO_2-brine duration (lower x-axis) and versus $\Delta t^{(G_{i-1})}$ the previous CO_2-gas duration (upper x-axis). Data are reported for experiments 1 (solid symbol) and 2 (open symbol).

Assuming a homogeneous distribution of calcite grains in the sample, calcite dissolution affects a 0.672 mm-thick zone on each side of the fracture where porosity ϕ increases from 0.07 to 0.32.

[13] Outlet Si concentration measured during the three first cycles indicates that Si is also steadily released during the CO_2-brine flow periods. Correlation between Si, K, and Ca peaks is observed when shifting from CO_2-gas to CO_2-brine flow. This indicates release of dissolved clay and/or clay particles, effluents being not filtered. The remaining release of Si, uncorrelated with K concentration during the CO_2-brine flow periods, is attributed to the dissolution of quartz grains (average size 15 μm). Integration of Si outlet concentration shows that approximately 4.4×10^{-4} cm^3 of quartz are dissolved, corresponding to the partial dissolution ($\sim$8 μm-thick layer) of the quartz grains at the fracture walls.

[14] The different dissolution of calcite and quartz, despite their similar proportion in the rock, is controlled by different kinetic constants [*Brady and Walther*, 1990; *Alkattan et al.*, 1998] and possible differences in reactive surface-areas of the two minerals.

4. Discussion

4.1. Matrix Porosity Changes

[15] Because quartz grains in contact with the fracture void are only partially dissolved, the reactive surfaces remain accessible to the CO_2-brine flow in the fracture. Conversely, the penetration of the calcite dissolution front in the claystone is larger than the calcite grain size. The mean position of the calcite dissolution front allows investigating whether calcite dissolution is controlled by dissolution kinetics or by the diffusion of the reactants in the clay matrix. Assuming diffusion in a semi-infinite medium, front penetration is $r = 2\sqrt{d_e t}$, where t is the elapsed time and $d_e = \phi^n d_m$ the effective diffusion coefficient with d_m the molecular diffusion coefficient and n the correction factor ($n > 1$) accounting for tortuosity and constrictivity of the diffusion paths in the matrix. Bromine diffusion experiments in the Tournemire claystone show that the effective diffusion coefficient $[d_e]_{Br} \approx 5.0 \times 10^{-12}$ $m^2.s^{-1}$ [*Savoye et al.*, 2006] yields a value of $n = 2 \pm 0.2$, with the molecular diffusion of Br in water $[d_m]_{Br} = 20.8 \times 10^{-10}$ $m^2.s^{-1}$. Consequently, with $[d_m]_{Ca} = 6 \times 10^{-10}$ $m^2.s^{-1}$, the position of the calcite dissolution front, perpendicular to the fracture, should be 2.9 ± 0.5 mm assuming diffusion only during the 4 CO_2-brine flow periods. This penetration is larger than the penetration distance evaluated by considering only the volume balance (i.e. r $\approx$ 0.672 mm), which indicate that calcite dissolution gradient is controlled by kinetics. While porosity increases in this altered zone due to progressive calcite dissolution, permeability of this altered zone does not change significantly as proved by the constant total sample permeability measured during CO_2-brine flow period. Accordingly, the increase of the hydraulic aperture between two cycles denotes an increase in the aperture gap only. It follows that the clay framework in the altered zone stays cohesive with nominally no swelling during CO_2-brine flow periods, despite the increase of porosity. In our case, swelling is mainly controlled by (i) the ionic strength of the flowing solution (I_S) compared to the ionic strength of the resident claystone pore fluid (I_P), assimilated here to the claystone-equilibrated fluid, (ii) the concentration in Ca and Mg that are expected to promote swelling of illite and smectite by cationic exchange. Here, osmotic swelling is low because $I_S > I_P$, and illite and smectite represent less than 10% of the rock volume.

4.2. Fracture Permeability Changes

[16] Fracture permeability remains unchanged during each CO_2-brine flow period. Conversely, permeability increases abruptly as soon as CO_2-brine replaces CO_2-gas. This permeability increase is associated with a sharp release of K, Si and Ca. Permeability increase is attributed to a fracture widening due to expelling a thin layer of clay particles as soon as CO_2-brine flow replaces CO_2-gas flow. This expelling cannot be attributed to mechanical stresses induced by the gas motion because the viscosity of the gas is hundred times lower than the viscosity of the brine.

[17] The fracture aperture variation $\Delta a_H^{(F_i - F_{i-1})} = a_H^{(F_i)} - a_H^{(F_{i-1})}$ occurs at the beginning of a CO_2-brine flow period F_i, and scales linearly with the duration $\Delta t^{(F_{i-1})}$ of the preceding CO_2-brine flow period F_{i-1}, independently of the duration of the CO_2-gas flowing period $\Delta t^{(G_{i-1})}$. The explanation is as follows: the volume of clay particles detached from fracture walls at the beginning of a given CO_2-brine flow period F_i, and consequently the associated change in the hydraulic aperture $\Delta a_H^{(F_i - F_{i-1})}$, are controlled by the thickness of the altered layer affected by clay decohesion during the previous CO_2-gas flow period (G_{i-1}). This thickness corresponds to the high porosity zone ($\phi > 40$–50%) where both calcite and quartz were dissolved during the preceding CO_2-brine flow period F_{i-1}. Because quartz dissolution kinetics is slower than calcite dissolution kinet-

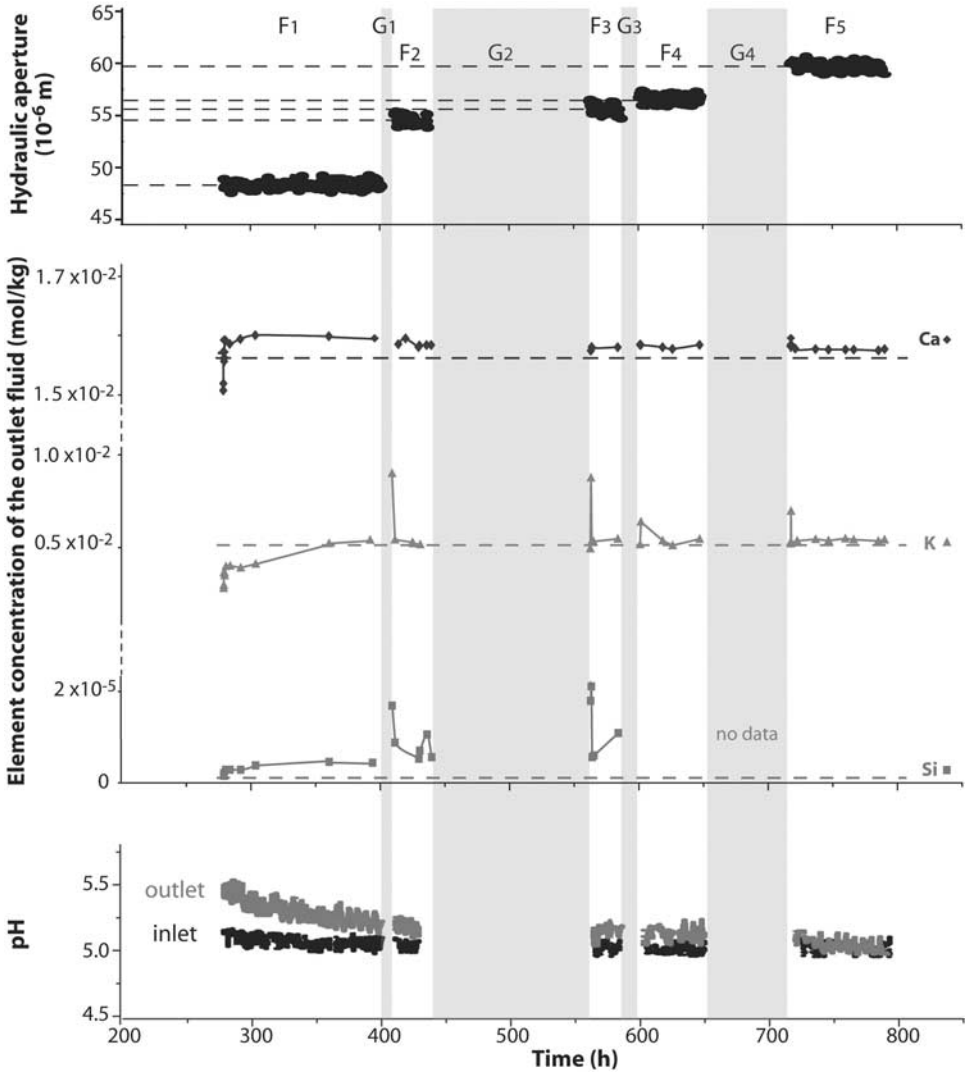

Figure 3. Summary of the parameters measured during the reactive percolation experiment in fractured claystone sample, starting after the saturation period (t = 280 hours). CO_2-brine injections are noted F_{1-5} and CO_2-gas injections are noted G_{1-4}. Horizontal dashed lines denote the brine concentration at the inlet (Table 1).

ics, the aperture increase is controlled by the quartz dissolution kinetics. Consequently, the linear relationship between the aperture increase and the duration of the preceding CO_2-brine flow period derives from the kinetically controlled quartz dissolution rate that scales as t^{-1}.

[18] Processes must be analyzed at nanometer scale in order to explain decohesion phenomenon. Strong adhesion stresses between clay particles are induced by a higher concentration of binding-cations at contacts points, whereas repulsive stresses prevail in interstices [*Jouanna et al.*, 2008]. Overall clay framework cohesion is maintained as long as attractive forces dominate. When CO_2 gas flows through the fracture, strong chemical gradients occur in the high porosity layer because of the infinite stock of CO_2 provided by the gas in the fracture gap, modifying the pore fluid speciation in the vicinity of clay particles contact points. Such decohesion process was experimentally observed by AFM tests for gypsum particles [*Plassard et al.*, 2005]. These authors show that attractive forces between particles were strongly dependent on the local value of the pH, with possible inversion from attractive to repulsive fields for small pH variations. At this point, we do not have the means to quantify this process in the case of the clay particles, but the experimental results presented here emphasize clearly the role of the CO_2-gas for modifying the cohesion properties of the clay particles. Figure 1c summarizes the proposed mechanisms controlling the fracture aperture increase.

5. Conclusions

[19] 1. Seepage of CO_2-brine and CO_2-gas can occur when diphasic mixture is trapped under a fractured caprock. This scenario is reproduced at laboratory scale. Results show that, for the studied claystone, the sole seepage of CO_2-brine through a fracture would not alter its permeability, while cycling flow of CO_2-gas and CO_2-brine increases fracture aperture and consequently the sample permeability.

[20] 2. Aperture increase is controlled by a twofold mechanism. First, calcite and, to a lesser extent, quartz

grains contained in claystone are dissolved by the CO_2-brine flow, thus creating an altered layer on fracture surface with a porosity of about 50%. Permeability of this altered zone is not significantly changed because clay particles (volume fraction >0.4) form a continuous framework. Second, CO_2-gas flow decreases the cohesion of clay particles that are subsequently transported by the next CO_2-brine flow. This decohesion is attributed to chemical-induced decrease of the attraction forces that links the clay particles.

[21] 3. Fracture widening after CO_2-gas flow is proportional to the amount of quartz dissolved that is in turn proportional to the previous aqueous fluid flow duration. Thus permeability may continue to rise discontinuously by such a process, unless antagonist processes (e.g. mechanical strain) reduce the fracture aperture.

[22] 4. Different values of P_{CO_2} and temperature ($T \leq 100°C$) should not affect the fracture widening process itself but would affect its rate by changing pH and dissolution rates. Conversely, different percentage of clay and carbonates, as well as different nature, shape and initial arrangement of clay particles are certainly critical parameters in view of extrapolation of the fracture widening mechanism to different claystones. For instance, *Noiriel et al.* [2007] show that when clay fraction is insufficient to form a continuous framework (volume fraction <0.2), fracture aperture may increase during CO_2-brine flow, while clay particle transported in the water may accumulate and eventually decrease the permeability.

[23] **Acknowledgments.** The authors wish to thank Sébastien Savoye and IRSN for providing the claystone sample as well as John P. Kaszuba and two anonymous reviewers for their useful comments to improve the manuscript.

References

Alkattan, N., E. H. Oelkers, J. L. Dandurand, and J. Schott (1998), An experimental study of calcite and limestone dissolution rate as a function of pH from −1 to 3 and temperature from 25 to 80°C, *Chem. Geol.*, *151*(1–4), 199–214.

Boisson, J.-Y., L. Bertrand, J.-F. Heitz, and Y. Moreau-Le Golvan (2001), In situ and laboratory investigations of fluid flow through an argillaceous formation at different scales of space and time, Tournemire tunnel, southern France, *Hydrogeol. J.*, *9*, 108–123.

Brady, P. V., and J. V. Walther (1990), Kinetics of quartz dissolution at low temperatures, *Chem. Geol.*, *82*, 253–264.

Gherardi, F., T. Xu, and K. Pruess (2007), Numerical modeling of self-limiting and self-enhancing caprock alteration induced by CO_2 storage in a depleted gas reservoir, *Chem. Geol.*, *244*, 103–129.

Hildenbrand, A., and B. M. Krooss (2003), CO_2 migration processes in argillaceous rocks: Pressure-driven volume flow and diffusion, *J. Geochem. Explor.*, *78–79*, 169–172, doi:10.1016/S0375-6742(03)00077-3.

Jouanna, P., L. Pèdesseau, G. Pèpe, and D. Mainprice (2008), Mass and momentum interface equilibrium by molecular modeling. Simulating AFM adhesion between (120) gypsum faces in a saturated solution and consequences on gypsum cohesion, *Cem. Concr. Res.*, *38*, 290–299.

Noiriel, C., B. Madé, and P. Gouze (2007), Impact of coating development on the hydraulic and transport properties in argillaceous limestone fracture, *Water Resour. Res.*, *43*, W09406, doi:10.1029/2006WR005379.

Plassard, C., E. Lesniewska, I. Pochard, and A. Nonat (2005), Nanoscale experimental investigation of particle interactions at the origin of the cohesion of cement, *Langmuir*, *21*, 7263–7270.

Pruess, K., and J. Garcia (2002), Multiphase flow dynamics during CO_2 injection into saline aquifers, *Environ. Geol.*, *42*, 282–295.

Sibai, M., F. Homand, and J. P. Henry (1993), Sondage CD du tunnel de Tournemire—Caractérisation des argilites, rapport technique, Lab. de Mec. des Solides, CEA, IPSN, Villeneuve d'Ascq, France.

Savoye, S., J.-L. Michelot, C. Wittebroodt, and M. V. Altinier (2006), Contribution of the diffusive exchange method to the characterization of pore-water in consolidated argillaceous rocks, *J. Contam. Hydrol.*, *86*, 87–104.

M. Andreani, P. Gouze, L. Luquot, and P. Jouanna, Géosciences Montpellier, CNRS, F-34095 Montpellier, France. (andreani@msem.univ-montp2.fr)